PROCEEDINGS OF SCIENCE

Impact Of Pairing Correlations On The Chemical Composition Of The Inner Crust Of A Neutron Star

A. Pastore*, **M. Shelley and C. Aa. Diget**
Department of Physics, University of York, Heslington, York, Y010 5DD, United Kingdom
E-mail: alessandro.pastore@york.ac.uk

We investigate the impact of the role of pairing correlation on the energy per particles of Wigner-Seitz cells in the inner crust of a neutron star. In particular, we compare some common approximations done to treat pairing effects and we estimate the possible error. To reduce the computational cost of the calculations required to determine the chemical composition of the crust, we present a new numerical method based on Gaussian Emulator Process.

The 26th International Nuclear Physics Conference
11-16 September, 2016
Adelaide, Australia

*Speaker.

PoS(INPC2016)145

1. Introduction

Neutron stars are extreme astrophysical objects, with incredibly strong gravitational and magnetic fields, and densities second only to those of black holes. They are usually formed after the death of massive stars via type II supernovae. The density ranges from far greater than atomic densities ($\rho_b = 10^6 gcm^{-3}$ near the surface) to well above normal nuclear densities ($\rho_b = 3 \times 10^{15} gcm^{-3}$ in the core of the largest neutron stars), such is the effect of gravity for massive enough stars [1].

Following standard models [2], we can identify three major regions of the star: the outer crust, the inner crust and the core. Within the outer crust, we find neutron rich nuclei arranged in crystal lattice and surrounded by an electron gas [3]. By increasing the density, the proton-neutron asymmetry increases and neutrons start to drip-out forming a continuum gas [4]. For barionic densities ranging from $\rho_b \approx 5 \times 10^{11}$ g/cm^3 to $\rho_b \approx 2 \times 10^{14}$ g/cm^3, we define the inner crust: a region of the star where very exotic nuclei exist immersed in a neutron and electron gas. For higher values of the density, it is no more possible to form bound systems and the matter dissolves into a uniform Fermi liquid.

The inner crust represents a major challenge for nuclear-structure models. To describe such a region, the tool of choice is the Nuclear Energy Density Functional theory (NEDF) since it ables to describe with very high level of accuracy nuclear observables from drip-line to drip-line and to light to heavy systems [5, 6]. Since the seminal work of Negele and Vautherin [7], several groups have tried to determine the chemical composition of the inner crust by using microscopic functionals [8, 9, 10, 11]. In most cases, the authors have spotted the major difficulty of solving the corresponding microscopic Hartree-Fock-Bogoliubov equations due to numerical errors and computational cost. To overcome these difficulties some approximations are introduced: a very common one is to make use of semi-classic approximations [12] based on Thomas-Fermi approximations.

In the present article, we briefly discuss some of the common approximations used in microscopic calculations of the inner crust and we compare the resulting error. This is illustrated in Sec. 2. Determining the chemical composition of the inner crust at different values of density and eventually temperature is computationally demanding task, thus we present for the very first time a new method based on Gaussian Process Emulators (GPEs) to speed up the optimisation procedure. Some simple examples are discussed in Sec.3. In Sec.4, we present our conclusions.

2. Error estimate

To determine the cluster composition of the inner crust, we have to determine the minimal energy configuration of each Wigner-Seitz (WS) cell for a given barionic density and, eventually, temperature T [7]. Within the NEDF formalism, this means solving several Hartree-Fock-Bogoliubov (HFB) [13] problems for different cluster configurations and WS cells to identify the configuration at minimal energy. The correct treatment of the problem, would imply the solution of the HFB equations together with periodic boundary conditions (BC) [14]. This is very demanding from the computational point of view, thus a first simplification consists in adopting simpler BC, namely the Dirichlet-Neumann BC as detailed in Ref. [7]. This choice implies a discretisation of the neutron gas state and the appearance of possible spurious shell effects that could affect the results, as spotted In Ref. [15].

To better quantify the impact of spurious shell effects in HFB calculations, the authors of Ref. [16] compared the binding energy per nucleon, $\frac{E_n}{N}$, for a gas of free neutrons in a box of radius R_B and the analytical result coming from the equation of state (EoS) of a piece of pure neutron matter (PNM), $\frac{E_a}{N}$ [17].We define the energy difference due to the discretisation effects as

$$\delta e = \left| \frac{E_a}{N} - \frac{E_n}{N} \right| , \tag{2.1}$$

the quantity δe quantifies the accuracy of the calculations as a function of the box size.

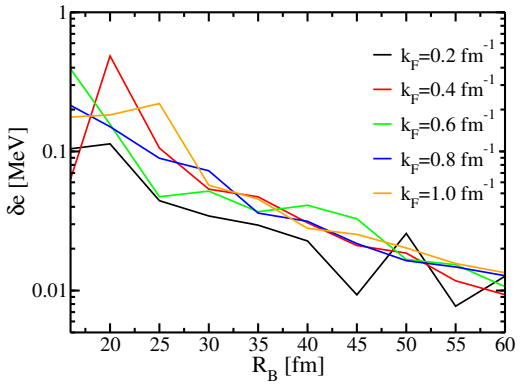

Figure 1: (Colors online) Evolution of the error δe on the energy per particle in PNM, Eq.2.1, as a function of the size of the box used to perform the calculations and different values of Fermi momentum k_F. See text for details

In Fig.1, we represent the results we obtained with our numerical code and using the SLy4 functional. As expected the error decreases as the box increases with very small dependence on the value of the density of the system ρ_n, here expressed in terms of Fermi momentum $k_F = (3\pi^2\rho_n)^{1/3}$. We observe that the discrepancy between the two calculations can be very small, $\approx$10 keV, for large boxes ($R_B = 60$ fm) and thus corresponding to the low-density region of the crust, while for small boxes $R_B\approx$20 fm, corresponding to the high density region, such a discrepancy can be of the order of $\approx$ 200 keV. We can fit these results via a simple function as

$$\sigma_{finite}(R_{WS}) = \frac{a}{R_{WS}^2} , \tag{2.2}$$

to estimate the error done for each WS calculation. The parameter $a = 61.67$ fm^2 has been fitted on the data shown in Fig.1. Using this function, we obtain the finite-size error related to each HFB calculations done for the different WS cells. For the current work, we use the WS cells extracted from the original work of Negele and Vautherin [7] and given in Tab.1. In the present article, we discard the denser configurations, ^{1500}Zr and ^{982}Ge, since they are not stable in our HFB calculations as discussed in Ref. [18].

To avoid this problem, several authors prefer to adopt semi-classical approximations [12, 19, 20, 11]. In most of the calculations, pairing properties are simply neglected or treated at the simpler

Zone	Z	N	R_{WS} [fm]
11	40	140	53.6
10	40	160	49.2
9	40	210	46.4
8	40	280	44.4
7	40	460	42.2
6	50	900	39.3
5	50	1050	35.7
4	50	1300	33.0
3	50	1750	27.6
2	40	1460	19.6
1	32	950	14.4

Table 1: Composition of the inner crust according to the work of Negele and Vautherin [7]. Each cell is characterised by a given proton (Z) and neutron (N) number and a fixed WS radius R_{WS}.

BCS level [21]. Pairing correlations play a major role in determining the crust composition [9], thus it is very important to assess the impact of such an approximation on the actual semi-classic calculations.

To assess the quality of the different approximation on the treatment of the pairing correlations, we performed different HFB calculations for the WS shown in Tab.1. For our test, we use the SLy4 functional in the *particle-hole* channel and a density dependent contact interaction in the *particle-particle* channel of the form

$$v^q(\mathbf{r}_1,\mathbf{r}_2) = V_0^q \left[1 - 0.7 \left(\frac{\rho_b\left(\frac{\mathbf{r}_1+\mathbf{r}_2}{2}\right)}{\rho_0} \right)^{0.45} \right] \delta(\mathbf{r}_1-\mathbf{r}_2) \, , \tag{2.3}$$

where $q = n, p$ is the isospin index and $\rho_0 = 0.16$ fm^{-3} and $V_0^q = -430$ MeVfm^3 together with a sharp cut off of 60 MeV in quasi-particle space. More details on the numerical methods used to solve HFB equations can be found in Refs. [18, 22, 23]. From each HFB calculation we extract the total energy per particle $\frac{E}{A}\big|_{HFB}$ and we compare it with the three different approximations

- A fully self-consistent Hartree-Fock (HF).
- A fully self-consistent Hartree-Fock plus the pairing condensation energy E_C [24] of the external neutron gas.
- A fully self-consistent Hartree-Fock+BCS calculation. See Ref. [23] for details.

We define three errors, as energy difference between the full HFB calculation and the Hartree-Fock one, σ_{HF}, the HF corrected by pairing condensation energy σ_{HF+C} and the HF-BCS one σ_{BCS}. Since the calculations are done in the same box, we assume that the error related to discretisation effect is roughly the same in the two calculations and thus it cancels out. This is of course a crude approximation, but we aim at estimating only the order of magnitude of the errors. The results

are illustrated in Fig.2 together with the error due to finite-size effects. We notice that although several authors claimed that HFB calculations are biased by spurious finite-size effects, the other approximations are also affected by a significant error, especially in the pure HF limit, when pairing properties are neglected. This error becomes more and more important in the regions of the crust where pairing correlations are at their maximum. The inclusion of pairing condensation energy E_C clearly improves the situation leading to errors comparable or smaller than the one related to finite-size effects. Only including fully self-consistently pairing correlations, although at BCS level, it is possible to bring down such an error to the order of few keV per particle. Notice that in Fig.2, the errors related to the BCS approximations have been multiplied by a factor of 5 to make them visible on the energy scale adopted in the figure.

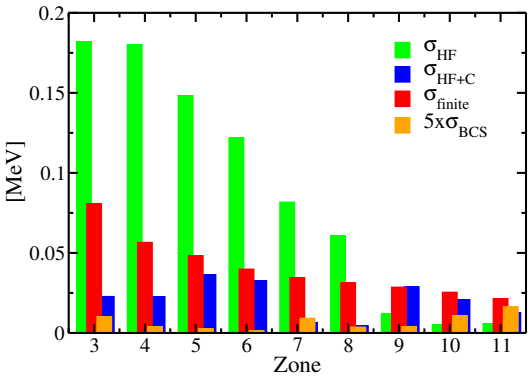

Figure 2: (Colors online) Estimated error of different approximations used to perform WS calculations. The zone number refers to the different WS as given in Tab. 1. See text for details.

The current analysis strongly depends on the choice of the pairing functional, for the current article, we have used a functional that gives a maximum pairing gap of 3.5 MeV in PNM as illustrated in Fig.5 of Ref. [18]. Weaker pairing strengths would lead to smaller errors. Since the calculations are usually done at fixed barionic density, it is not correct to assume that pairing correlations will be similar for different WS configurations, since the density of the external neutron gas is not constant. As a consequence, the errors presented in Fig.2, should be also taken into account in the minimisation procedure.

3. Gaussian Process Emulators

GPEs perform spatial interpolation for a sample of simulation outputs, by making probabilistic predictions based on this sample. This is a Bayesian approach to interpolation, also known as *Kriging*; it aims to extract the maximum amount of information possible about the surface being simulated. The emulator *learns* about the simulation, building its own model, which is improved by each extra simulation output it receives. GPEs work best for deterministic simulations, where the same input parameters give a consistent output. It is also important that the output varies

smoothly with the input parameters. GPEs can be used if the simulation output is non-exact (has an associated non-random error), as is the case with any HFB calculations.

The motivation for using GPEs is to reduce the computational burden for calculations of the inner crust composition. A GPE can emulate a simulation output, ideally with good accuracy, and in less time. This is particularly important in combination with an HFB solver that requires a remarkable amount of CPU time to describe WS cells.

The computational performance of the GPEs depends on the number of input data points. As long as the time taken to run the emulation is small compared with the simulation time, and an effective speedup is obtained, the use of the GPE will have been successful. The emulator must invert a covariance matrix, a process which does not scale linearly with the number of data points. However this is not a problem, even for millions of data points, since the time for this matrix inversion will still be dwarfed by the HFB calculation time.

There are a few ways of taking simulation output samples to give to the emulator. One can choose a grid of varying size, *e.g.* taking every 5th point along each dimension of the surface. Another method is Latin Hypercube (LHC) sampling. This divides the surface into equal chunks of a given size, and then selects randomly a point from within each chunk. This semi-random sampling provides a better coverage of the surface, and tends to produce a smaller overall error when compared with simple grid sampling.

GPEs can be used iteratively, once after each simulation output has been received, to intelligently choose points to calculate. After a given iteration, the emulator identifies the point on the surface with the greatest uncertainty, and the simulation then calculates this point. This is a *greedy*, but effective method for maximising the information gleaned while minimising the number of simulation runs. An improvement on this iterative method was proposed by Hoang *et al.* [25]. Here, the emulator tries to balance choosing points which minimise global error, with choosing points that continue to train the emulator, providing a more accurate emulation in the long term. This is known as *nonmyopic* (literally 'not-short-sighted') learning.

GPEs have been used in several areas of science, but never before in theoretical nuclear physics. They have been applied to atmospheric chemistry, as well as to studies into tsunamis around small islands [26], and models for Rabies [27]. The potential applications for GPEs are far-reaching. They will help in any situation where a large number of expensive computational simulations need to be carried out, so long as there is a correlation between these simulation outputs.

In Figure 3, we shows how a GPE could be applied to a one dimension simulation. We consider a test function $y(x)$, represented on the figure with dots, from which we extract some points with some random noise: 10 on the left panel and 20 on the right one. We assume for simplicity that each point comes with a constant error bar fixed by the user and not related to the way the points have been generated. We recall that in real applications, the underlying function $y(x)$ is not known and the way the points are extracted, either numerically or experimentally, may contain errors arising from different sources. We apply GPE to both sets of data. The interpolating function is shown as solid line. On the same figure we also represent the 95% confidence interval for both cases.

By comparing the results of the two data sets, we observe that the GPE provides an accurate prediction of the unknown function. The size of the 95% confidence interval decreases noticeably once we double the number of data points, but in both cases the GPE prediction still lies well

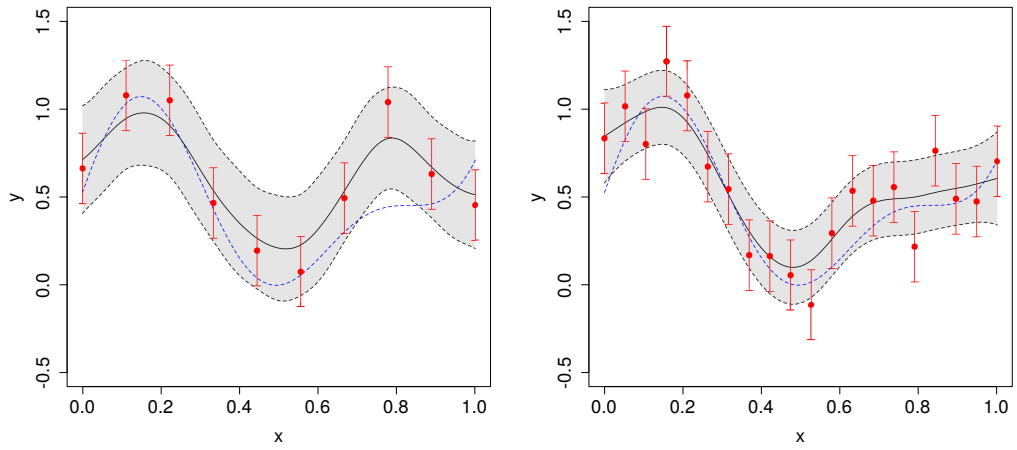

Figure 3: (Colors online) Demonstration of GPE applied to sample of 10 data points (left panel) and 20 data points (right panel). The dotted line represents the true unknown function, $y(x)$, evaluated at all values of x from 0 to 1 (arbitrary units). The points (with error bars) are the outputs of a simulation which is trying to reproduce this unknown function. These are the data points given to the GPE. The solid lines represent the outputs from the GPE. The shaded area represents the 95% confidence interval for the GPE output. See text for details.

within this interval for the majority of the input space. The largest discrepancy between emulation and true function happens at the boundaries, where there is less information for the GPE to use. Therefore, it can be useful to run the simulation for values slightly outside the region of interest, in order to help the GPE within the region of interest. For a more complex function, more points are needed to have the same quality of emulation. As a future development of GPEs, we aim at using them to simulate the energy landscape of different clusters at β-equilibrium and different barionic densities [7]. These results will be presented in a forthcoming publication.

4. Conclusions

In the present article, we have presented a preliminary study to estimate the error of different models for the calculation of the chemical composition of the inner crust of a NS. In particular, we have studied the impact of the use of Dirichlet-Neumann boundary conditions in HFB calculations and several common approximations to treat pairing correlations. We have observed that, despite common statements, the error for different WS cells arising from finite-size effects or neglecting pairing correlations is of the same order of magnitude. This aspect has not been fully explored in semi-classical methods and it should be clearly addressed in the future since such an error is one or two order of magnitude larger than the typical energy differences between the different cluster configurations. A simple way to reduce this error is to consider the contribution of pairing condensation energy of the neutron gas. In this case the errors in the calculations are comparable or even smaller than the one related to finite-size effects. The inclusion of pairing condensation energy is not computationally expensive and it could be easily improved via a simple Local Density

Approximation to take into account the enhancement/reduction of pairing correlations around the nuclear cluster [18].

Since the WS cell is composed by a cluster immersed in a neutron gas, once could expect that a simple BCS approximation could be enough to discuss pairing correlations [23, 28]. We have thus compared fully self-consistent HFB and BCS calculation showing that the discrepancy on the energy per particle of the two calculations is very small. We thus conclude that semi-classical methods can be considered competitive respect to complete HFB calculations in a box, only if pairing correlations are taken properly into account.

In the second part of the article, we introduce a new statistical method called Gaussian Process Emulator to reduce the computational cost in numerical calculations done to determine the cluster composition of the crust, independently from the adopted method (either semi-classical ones or quantal). The main advantage of the GPE method is the possibility of taking into account the presence of error bars to determine the energy surfaces leading to the cluster composition. We plan to combine the GPE method with improved HFB solver together with currently estimated error bars to determine the chemical composition of the inner crust for few selected Skyrme functionals.

References

[1] N. Chamel and P. Haensel, *Physics of neutron star crusts*, *Living Reviews in Relativity* **11** (2008) .

[2] P. Haensel, A. Y. Potekhin and D. G. Yakovlev, *Neutron stars 1: Equation of state and structure*, vol. 326. Springer Science & Business Media, 2007.

[3] J. Pearson, S. Goriely and N. Chamel, *Properties of the outer crust of neutron stars from hartree-fock-bogoliubov mass models*, *Physical Review C* **83** (2011) 065810.

[4] N. Chamel, A. Fantina, J. L. Zdunik and P. Haensel, *Neutron drip transition in accreting and nonaccreting neutron star crusts*, *Physical Review C* **91** (2015) 055803.

[5] M. Bender, P.-H. Heenen and P.-G. Reinhard, *Self-consistent mean-field models for nuclear structure*, *Reviews of Modern Physics* **75** (2003) 121.

[6] S. Goriely, N. Chamel and J. Pearson, *Skyrme-hartree-fock-bogoliubov nuclear mass formulas: Crossing the 0.6 mev accuracy threshold with microscopically deduced pairing*, *Physical review letters* **102** (2009) 152503.

[7] J. Negele and D. Vautherin, *Neutron star matter at sub-nuclear densities*, *Nuclear Physics A* **207** (1973) 298–320.

[8] M. Baldo, E. Saperstein and S. Tolokonnikov, *A realistic model of superfluidity in the neutron star inner crust*, *The European Physical Journal A* **32** (2007) 97–108.

[9] F. Grill, J. Margueron and N. Sandulescu, *Cluster structure of the inner crust of neutron stars in the hartree-fock-bogoliubov approach*, *Physical Review C* **84** (2011) 065801.

[10] J. Pearson, N. Chamel, S. Goriely and C. Ducoin, *Inner crust of neutron stars with mass-fitted skyrme functionals*, *Physical Review C* **85** (2012) 065803.

[11] B. Sharma, M. Centelles, X. Vinas, M. Baldo and G. Burgio, *Unified equation of state for neutron stars on a microscopic basis*, *Astronomy & Astrophysics* **584** (2015) A103.

[12] M. Brack, C. Guet and H.-B. Hakansson, *Selfconsistent semiclassical description of average nuclear bulk properties-a link between microscopic and macroscopic models*, *Physics Reports* **123** (1985) 275–364.

[13] P. Ring and P. Schuck, *The nuclear many-body problem*. Springer Science & Business Media, 2004.

[14] N. Chamel, *Neutron conduction in the inner crust of a neutron star in the framework of the band theory of solids*, *Physical Review C* **85** (2012) 035801.

[15] M. Baldo, E. Saperstein and S. Tolokonnikov, *The role of the boundary conditions in the wigner–seitz approximation applied to the neutron star inner crust*, *Nuclear Physics A* **775** (2006) 235–244.

[16] J. Margueron, N. Van Giai and N. Sandulescu, *Proceedings of the international symposium exoct07*, .

[17] D. Davesne, A. Pastore and J. Navarro, *Extended skyrme equation of state in asymmetric nuclear matter*, *Astronomy & Astrophysics* **585** (2016) A83.

[18] A. Pastore, S. Baroni and C. Losa, *Superfluid properties of the inner crust of neutron stars*, *Physical Review C* **84** (2011) 065807.

[19] F. Douchin and P. Haensel, *A unified equation of state of dense matter and neutron star structure*, *Astronomy & Astrophysics* **380** (2001) 151–167.

[20] J. Pearson, N. Chamel, A. Pastore and S. Goriely, *Role of proton pairing in a semimicroscopic treatment of the inner crust of neutron stars*, *Physical Review C* **91** (2015) 018801.

[21] X. Viñas, P. Schuck and M. Farine, *Thomas-fermi approximation to pairing in finite fermi systems. the weak coupling regime*, in *Journal of Physics: Conference Series*, vol. 321, p. 012024, IOP Publishing, 2011.

[22] A. Pastore, *Superfluid properties of the inner crust of neutron stars. ii. wigner-seitz cells at finite temperature*, *Physical Review C* **86** (2012) 065802.

[23] A. Pastore, J. Margueron, P. Schuck and X. Viñas, *Pairing in exotic neutron-rich nuclei near the drip line and in the crust of neutron stars*, *Physical Review C* **88** (2013) 034314.

[24] R. Haslinger and A. V. Chubukov, *Condensation energy in strongly coupled superconductors*, *Phys. Rev. B* **68** (Dec, 2003) 214508.

[25] T. N. Hoang, K. H. Low, P. Jaillet and M. Kankanhalli, *NonmyopicâĹĹ-bayes-optimal active learning of gaussian processes*, in *Proc. ICML*, pp. 739–747, 2014.

[26] T. S. Stefanakis, E. Contal, N. Vayatis, F. Dias and C. E. Synolakis, *Can small islands protect nearby coasts from tsunamis? An active experimental design approach*, *Proceedings of the Royal Society of London Series A* **470** (Nov., 2014) 20140575–20140575, [1305.7385].

[27] A. Boukouvalas, D. Cornford and A. Singer, *Managing uncertainty in complex stochastic models: Design and emulation of a rabies model*, in *6th St. Petersburg Workshop on Simulation*, pp. 839–841, 2009.

[28] A. Pastore, *Pairing properties of the inner crust of neutron stars at finite temperature*, in *EPJ web of conferences*, vol. 66, p. 07019, EDP Sciences, 2014.